

Vertical profiling of tropical precipitation using passive microwave observations and its implications regarding the crash of AF447

Ziad S. Haddad
Jet Propulsion Laboratory, California Institute of Technology
and
Kyung-Won Park
Joint Institute for Regional Earth System Science and Engineering, UCLA

Abstract

In a recent study (Haddad and Park, 2009), a method was proposed to use co-located simultaneous observations by the space-borne Tropical Rainfall Measuring Mission (TRMM) precipitation radar and microwave imager to train the microwave radiometer to retrieve vertical profiles of precipitation in the absence of radar observations. This radar-trained passive-microwave approach was developed for mid-latitude precipitation regimes, where it was found that the inhomogeneity of the rain within the radiometer field of view was the main impediment to the estimation of the vertical distribution of rain. The approach constrains the brightness-temperature combinations used in the retrieval to lie in the orthogonal complement to the two main clear-sky principal components in brightness-temperature space. This note summarizes the results of applying this approach to observations over the Atlantic Inter-Tropical Convergence Zone during May 2009, and deriving estimates of the uncertainty in passive-microwave retrievals of the storm-top height and of the first vertical principal component of the rain. The results are illustrated on a serendipitous granule of data taken while the TRMM radar was unfortunately not operational, about twenty minutes after the last transmission from the ill-fated flight AF447.

1. Introduction

Two space-borne radars capable of measuring vertical profiles of precipitation are currently orbiting Earth: the Tropical Rainfall Measuring Mission's Precipitation Radar (TRMM PR), and CloudSat's Cloud Profiling Radar (CPR). The sampling frequency of both instruments is poor: TRMM's cross-track-scanning PR has a surface-clutter-limited swath of about 220 km, which results in a revisit frequency of about once every three days on average for points near the equator; CPR does not scan at all, and its sun-synchronous orbit has a ground revisit time of 16 days. Different approaches have been proposed to use the observations of these radars and train microwave radiometers to retrieve precipitation fields at times and locations where no radar data is available, including Masunaga and Kummerow, 2005, Grecu and Olson, 2006, Jiang and Zipser, 2006, Viltard et al, 2006, and Haddad and Park, 2009. The latter approach, to which we shall refer in this paper as HP09, specifically aims at retrieving the main parameters governing the vertical distribution of precipitation, and was evaluated over five different regions in the mid-latitudes. In HP09, we showed how a naive direct Bayesian retrieval of

vertical structure via principal components produces very mixed results, how a mildly careful segmentation of the pixels according to an 85GHz-derived simple measure of inhomogeneity highlights that the problem is with the observations where the field of view encompasses precipitation as well as clear-air sea surface, and finally that the proposed approach dramatically improves the retrievals in the partial-clear-surface category. This report describes new results using the approach in the case of tropical convection. Section 2 summarizes the steps of the approach, and section 3 describes the resulting retrieval algorithm for data gathered over the Atlantic Inter-Tropical Convergence Zone (ITCZ) during May 2009, with estimates of the uncertainty in passive-microwave retrievals of the storm-top height and of the first vertical principal component of the rain. Finally, section 4 illustrates the results with a particularly interesting case where only radiometer measurements were available, namely a serendipitous granule of TRMM data taken over the Atlantic ITCZ about twenty minutes after the last transmission from the ill-fated flight AF447 on June 1, 2009.

2. Deriving radiometer retrievals using joint radar/radiometer observations

Since radiometer estimates of the rain rate “at the surface” are no more or less credible than radiometer estimates at any discrete altitude (radiometers do not directly measure the rain rate at any specific height), the approach that we took in HP09 is first to characterize the vertical variability of the precipitation by appropriately transforming the radar-derived vertical radar precipitation-rate profiles, on one hand, and try to estimate the main modes of this variability from the simultaneously-measured brightness temperatures. In our implementation, over a given region and a given season (defined so the precipitation events can be viewed as samples from the same rain regime), the first step of this approach is the calculation of the principal components P_1', \dots, P_{60}' of the estimated vertical precipitation-rate vector $\underline{P} = (P_1, \dots, P_{60})$ over pixels that consist of 3x3 contiguous radar fields-of-view, representing a footprint of about 15x15 km² in the case of TRMM PR and its current nominal altitude of about 402 km. We keep the first sixty 250-m vertical range bins out of the eighty-bin TRMM level-2 profiles in order not to include, in the principal components analysis (PCA), variables which will be zero in all but a handful of radar beams over the sampled region and season. Call U the orthogonal change-of-basis matrix, $\underline{P}' = U \underline{P}$, and for future reference call μ_i the mean of P_i' .

Previous analyses have shown that the first three principal components typically capture over 90% of the variability in \underline{P} (see e.g. Coppens et al, 2000, and HP09). Assuming that this is the case in the region/season at hand, the approach is to build a database B containing samples $(P_1'(n), P_2'(n), P_3'(n); T_1(n), \dots, T_9(n))$ of the first three principal components of the radar-estimated precipitation together with the 9 simultaneous measurements of the brightness temperature in each of the 9 TRMM Microwave Radiometer (TMI) channels, with the index “n” tracking the sample number. This database can then be used to make retrievals in the absence of any radar measurements: indeed, given a vector of radiometer measurements \underline{T} , one can calculate the 3 conditional means

$$\hat{P}_i = \frac{1}{K} \sum_n P_i'(n) e^{-0.5(\bar{T}(n)-\underline{T})' C^{-1} (\bar{T}(n)-\underline{T})}, \quad i = 1, 2 \text{ or } 3 \quad (1)$$

in which K is the normalizing constant $K = \sum_n \exp[-0.5(\vec{T}(n) - \underline{T})' C^{-1}(\vec{T}(n) - \underline{T})]$, and C is the sum of the observation error variance in \underline{T} (a diagonal matrix) and the conditional covariance matrix of \vec{T} given \underline{T} . The corresponding estimate of the vertical precipitation-rate vector \underline{P} is then

$$\underline{P} = U' \begin{pmatrix} \hat{P}_1 \\ \hat{P}_2 \\ \hat{P}_3 \\ \mu_4 \\ \cdot \\ \cdot \\ \cdot \\ \mu_{60} \end{pmatrix} \quad (2)$$

where U' is the transpose of U .

In HP09, it was shown that this approach is successful in rain regimes where the precipitation typically fills the radiometer beams, and fails when a significant portion of the radiometer field of view sees the surface free of precipitation. In other words, the approach fails when the brightness temperatures in the database are biased by the contribution from the clear-sky surface in a significant portion of the beam. Our solution is to modify the approach to neutralize as much as possible the signature of the surface, in a way that is similar in inspiration to the scattering-index approach taken by Grody (1991). This is accomplished by first performing a principal component analysis of the brightness temperature vector in clear air, where the radiances are sensitive mainly to the surface emissivity, itself a function of two variables, the near-surface wind and column water vapor (itself correlated with sea surface temperature – see e.g. Petty, 1994). One would therefore expect that, of the 9 clear-sky principal components of the brightness temperatures, 7 would have relatively small variances. It is therefore natural to modify our approach so that, instead of using all 9 brightness temperatures T_1, \dots, T_9 in our estimate (1) of the conditional expectation of P_1', P_2' and P_3' , we use instead only the 7 smaller clear-sky brightness-temperature principal components $\underline{T}' = (T_3', \dots, T_9')$. The approach is to use (2) to estimate the conditional expectation of \underline{P} , with

$$\hat{P}_i = \frac{1}{K} \sum_n P_i'(n) e^{-0.5(\vec{T}'(n) - \underline{T}')' C'^{-1}(\vec{T}'(n) - \underline{T}')}, \quad i = 1, 2 \text{ or } 3 \quad (1')$$

where C' is the 7x7 error covariance matrix of \underline{T}' . As we note in HP09, this approach may not be optimal for several reasons: foremost, it treats the radar-estimated vertical profiles of precipitation as the reference against which the passive measurements are to be trained – this is a shortcoming because the radar-derived profiles do not constitute absolute truth; perhaps most important, we performed the principal component analyses on the rain rates and the brightness temperatures themselves, tacitly implying that Gaussian statistics govern the joint behavior of these variables, when it is not necessarily true that the marginal distributions are normal, let alone the joint density functions. On the other hand, the approach does allow one to estimate, from the radiometer measurements alone, any radar-derived variable, by calculating the corresponding

conditional mean as given by (1'). In particular, since TRMM PR has a nominal detection threshold of about 17 dBZ (see e.g. Takahashi and Iguchi, 2008), one can estimate the 17-dBZ storm-top height \hat{h} using

$$\hat{h} = \frac{1}{K} \sum_n h(n) e^{-0.5(\bar{T}'(n)-\underline{T}')' C'^{-1} (\bar{T}'(n)-\underline{T}')}, \quad (1'')$$

in which $h(n)$ is the radar-detected 17-dBZ storm-top height of the n^{th} sample in the database. It is useful to note that the r.m.s. uncertainty σ in the retrieved values of \hat{h} can be estimated using the conditional variance

$$\sigma^2 = \frac{1}{K} \sum_n [h(n) - \hat{h}]^2 e^{-0.5(\bar{T}'(n)-\underline{T}')' C'^{-1} (\bar{T}'(n)-\underline{T}')}, \quad (3)$$

a procedure that allows one to place error bars on all radiometer-only estimates produced by this approach.

3. Retrievals for the Atlantic Inter-tropical Convergence Zone in May 2009

These considerations were applied to the database constructed from the TRMM radiometer and radar data observed over the rectangular region lying between 45°W and 15°W, from the equator to 5°N, from May 1 to May 29, 2009. TRMM PR experienced an instrument anomaly on May 29 resulting in missing data starting with orbit 65716, but we can nevertheless consider this database to be representative of the conditions that prevailed over the ITCZ during May. Table 1 shows the coefficients of the first principal component P_1' of the radar-derived vertical precipitation-rate vector (P_1, \dots, P_{60}) with the components expressed in mm/hr: the first 14 coefficients, from the surface up to 3.5 km, have values between 0.2 and 0.3, and decrease to 0 as the height bin number increases up to the maximum 15 km. Thus P_1' is essentially an average of the rain rate in the first 14 height bins representing the 3500 meters above the surface, with a normalization constant of approximately 0.25 instead of 1/14. Since $14 \times 0.25 = 3.5$, one can consider that $P_1' \approx 3.5 \times \text{mean-rain-rate mm/hr}$, the mean being over the lowest 3500 meters and over the $15 \times 15 \text{ km}^2$ approximate area of the pixel. Thus a value of $P_1' = 70$ is approximately equivalent to an average rain rate of 20 mm/hr in the lowest 3.5 km above the 225 km^2 surface. Table 2 shows the coefficients of the second principal component: it is approximately the difference between the average precipitation rate near the surface (i.e. over the bottom 1.75 km) and that above 2 km (with a weighting function that remains significant well above the freezing level). The main difference between these modes and the principal components calculated for the 5 regions in HP09 is that the first principal component P_1' in the present case captures 93% of the variability, while the P_2' accounts for another 3.3%. This implies that if we can estimate these two principal components, we can reconstruct the vertical precipitation profiles (using (2) as in section 2) without increasing the uncertainty by more than about 3.7%. Figure 1 illustrates the extent to which the first two principal components determine the vertical distribution of the precipitation by plotting the profiles in our database that lie at the four extremities of our domain in (P_1', P_2') space.

To implement the retrieval procedure, we need to derive the clear-sky principal components of the brightness temperatures. The analysis of all database samples for which the radar did not detect any precipitation, reveals that the first two principal

components capture respectively 85.8% and 5.8% of the clear-sky variability in the brightness temperatures. Table 3 shows the coefficients of the 7 remaining principal components. It is not straightforward to visualize the correlation between these 7 observables and the principal components of the precipitation. To verify that they are indeed correlated, we applied our Bayesian retrieval procedure as in the previous section, using as measurements each of a subset of points from the database to which we added realistic measurement noise. Specifically, consider the exponent in (1') as quantifying the normalized distance d between any two measurements in brightness-temperature space:

$$d^2 = (\vec{T}_1' - \vec{T}_2')^t C'^{-1} (\vec{T}_1' - \vec{T}_2') \quad (4)$$

We started by selecting, as test inputs, those samples which have at least four reasonably close neighbors in the database, i.e. for which $d^2 \leq 5$. The nominal value of 5 that we used for the radius was chosen somewhat arbitrarily, and can be interpreted as allowing the two points to differ by one noise standard deviation in each of 5 channels. The criterion guarantees that the samples that we use as test inputs are not isolated relative to the total population represented by the database. From each of these samples, we then generated 500 synthetic measurements by adding independent white Gaussian noise with a standard deviation of 1K to each of the nine channels. The synthetically noisy measurements were then used as inputs to the Bayesian retrieval, and the conditional means of the storm-top height and of the first two principal components of the precipitation were computed. The results are shown in figures 2 and 3. Note the “conservative” tendency of the conditional mean, to overestimate the values at the lower end of the range and to underestimate the values at the higher end, especially evident in the estimates of the second principal component. While this simulation is not the perfect way to quantify the uncertainty in our Bayesian procedure, the estimates of the first precipitation principal component in our simulation have an r.m.s. error that varies from a low of 1.18 for values of P_1' near 1 to a high of 7.7 for values of P_1' near 35. Similarly, the estimates of the radar-detected storm-top heights have an r.m.s. error between 0.27 km and 0.95 km. The error bars that we calculated are shown in green on figures 2 and 3.

4. Application to a TRMM granule from June 1, 2009

The main motivation for choosing May 2009 to illustrate our procedure is the TRMM orbit 65760, during which the spacecraft took data over an area that included the last confirmed coordinates of flight AF447, about 20 minutes after the last transmission from the ill-fated aircraft. As noted above, the TRMM radar was not taking data at that time, but the approach described above can be applied using the May 09 database of joint TRMM PR and TMI measurements over the Atlantic ITCZ. What information could this shed on the vertical structure of the precipitation in the area of interest?

We applied the procedure described in section 2, using the training database described in section 3, to the brightness temperatures measured on June 1 at 0230Z by the TMI during that portion of TRMM granule 65760 that intersected the rectangular region that defines our area of interest. Figure 4 shows the brightness temperatures measured in the V-polarized channels. Figure 5 shows the resulting estimates of the first principal component of the precipitation, and figure 6 shows the estimates of the storm-top heights. The last known position of flight AF447 falls in the center of the area of the most intense convection, with values of the first precipitation principal component equivalent to a

vertically-averaged rain rate of 20 mm/hr over the 3.5 km nearest the surface, and with storm-top heights exceeding 35000 ft. Such information about the vertical structure of the precipitation cannot be derived from the IR data that formed the backbone of the preliminary meteorological analysis that was commissioned by the cognizant aviation authority (BEA, 2009). Our TMI-based estimates support the conclusion, in the preliminary analysis, that the stormy activity in the area where the flight disappeared was not exceptional, when compared to typical ITCZ convective events. Nevertheless, our TMI-based estimates also identify that particular area as the portion of the storm with the most intense convective activity, with 17-dBZ storm-top heights exceeding the flight level of the aircraft (FL350).

5. Conclusions

As we concluded in our earlier study (HP09) that considered mid-latitudes precipitation regimes, our main conclusion in the case of tropical convection considered in the present application is that it is indeed possible to retrieve reasonably detailed information about the vertical distribution of precipitation from the measurements of a multi-frequency passive microwave radiometer such as TMI, using a database of simultaneous radar and radiometer measurements that is representative of the prevailing surface and atmospheric conditions. The approach is Bayesian, in that it estimates the conditional mean of the precipitation variables (whether the first vertical principal components of the precipitation rates or the storm-top height) using the radar+radiometer database as the sample joint probability distribution. To neutralize the effect of the radiometric signature of the surface on the portion of the radiometer beams that does not contain precipitation, the approach conditions the means on the small-eigenvalue principal components of the observed brightness temperatures, obtained from an analysis of the clear-sky measurements in the database, as was done in the original study (HP09). One reason this estimation procedure is not optimal is the fact that it uses principal components analyses of the vertical rain rate vector and of the vector of brightness temperatures over a given pixel – in spite of the fact that neither vector of random variables (the precipitation rates or the radiances) is normally distributed. These issues deserve more detailed examination, especially in light of the information about the vertical characteristics of precipitating clouds that multi-channel microwave radiometers can reveal, as illustrated by the example in section 4.

6. Acknowledgement

This work was performed at the Jet Propulsion Laboratory, California Institute of Technology, under contract with the National Aeronautics and Space Administration.

7. References

- BEA (Bureau d'Enquêtes et d'Analyses pour la sécurité de l'aviation civile), 2009: Rapport d'étape – Accident survenu le 1er juin 2009 à l'Airbus A330-203 immatriculé F-GZCP exploité par Air France vol AF 447 Rio de Janeiro – Paris, *available from* <http://www.bea.aero/docs/2009/f-cp090601e1/pdf/f-cp-0-6-1e1.pdf>
- Coppens, D., Z.S. Haddad and E. Im, 2000: Estimating the uncertainty in passive-microwave rain retrievals. *J. Atmos. Ocean. Tech.* **17**, 1618-1629.
- Greco, M., and W.S. Olson, 2006: Bayesian Estimation of Precipitation from Satellite Passive Microwave Observations Using Combined Radar-Radiometer Retrievals. *J. Appl. Met. Clim.* **45**, 416-433.
- Grody, N.C., 1991: Classification of snow cover and precipitation using the Special Sensor Microwave Imager. *J. Geophys. Res.* **96**, 7423-7435.
- Haddad, Z.S., and K.-Y. Park, 2009: Vertical profiling of precipitation using passive microwave observations: The main impediment and a proposed solution, *J. Geophys. Res.* **114**, D06118, DOI:10.1029/2008JD010744
- Jiang, H., and E. J. Zipser, 2006: Retrieval of hydrometeor profiles in tropical cyclones and convection from combined radar and radiometer observations. *J. Appl. Meteor.* **45**, 1096-1115.
- Masunaga, H., and C.D. Kummerow, 2005: Combined radar and radiometer analysis of precipitation profiles for a parametric retrieval algorithm. *J. Atmos. Ocean. Tech.* **22**, 909-929.
- Petty, G.W., 1994: Physical retrievals of over-ocean rain rate from multichannel microwave imagery. Part II: algorithm implementation. *Meteor. Atmos. Phys.* **54**, 101-122.
- Takahashi, N., and T. Iguchi, 2008: Characteristics of TRMM/PR System Noise and Their Application to the Rain Detection Algorithm. *IEEE T. Geosci. Rem. Sens.* **46**, 1697-1704.
- Viltard, N., C. Burlaud and C.D. Kummerow, 2006: Rain retrieval from TMI brightness temperature measurements using a TRMM PR-based database. *J. Appl. Meteor. Clim.* **45**, 455-466.

Figure Captions

Figure 1. Sample radar-retrieved profiles from our Atlantic ITCZ May'09 database that lie at the four corners of the (P_1', P_2') rain-profile principal-component space.

Figure 2. Estimated principal components of the precipitation (vertical axis), plotted against the actual values in our May'09 Atlantic ITCZ database (horizontal axis). Estimates were calculated after adding simulated measurement noise to the actual samples (shown in red) in the database.

Figure 3. Bayesian estimates of the 17-dBZ storm-top height (vertical axis), plotted against the actual storm-top heights in our May'09 Atlantic ITCZ database (horizontal axis). Estimates were calculated after adding simulated measurement noise to the actual samples (shown in red) in the database.

Figure 4. Brightness temperatures measured by the TRMM Microwave Imager on 1 June 2009 at 0230Z during orbit 65760: 10.7GHz-Vpol top left, 19.4GHz-Vpol top right, 21.3V center left, 37GHz-Vpol center right, 85.5GHz-Vpol bottom left.

Figure 5. First principal component (essentially 3.5 times the vertical average) of the rain-rate, estimated from TRMM Microwave Imager measurements taken on 1 June 2009 at 0230Z as in figure 4. Flight AF 447 had reached waypoint INTOL at 0133Z and estimated at that time that it would reach waypoint TASIL at 0223Z.

Figure 6. Estimates of the 17-dBZ storm-top heights using the same data as in figures 4 and 5. The last known position of flight AF 447 (BEA, 2009) places the aircraft at 2°58.8'N 30°35.4'W at 0210Z heading NE.

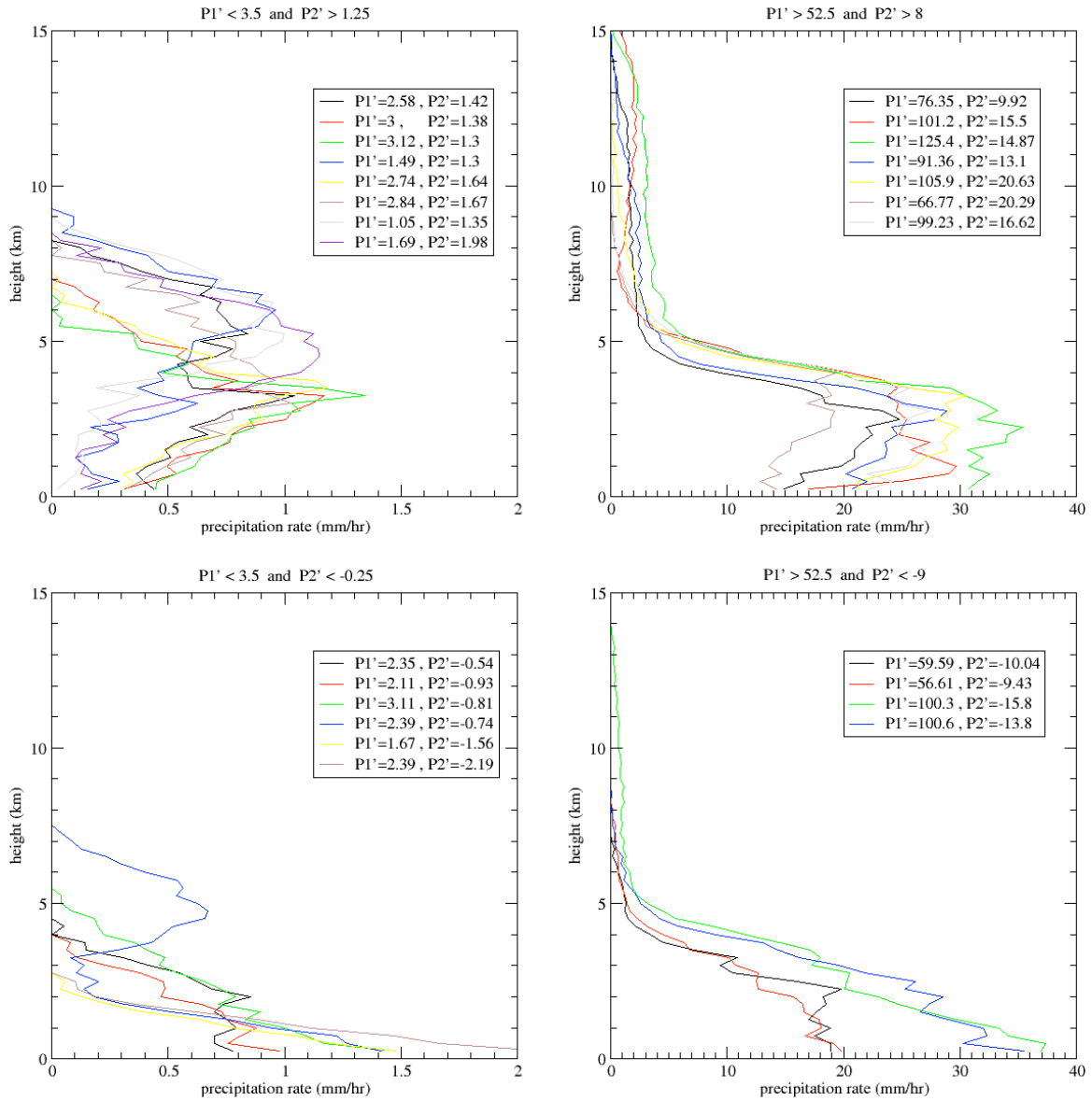


Figure 1. Sample radar-retrieved profiles from our May'09 Atlantic ITCZ database that lie at the four corners of the (P_1', P_2') rain-profile principal-component space.

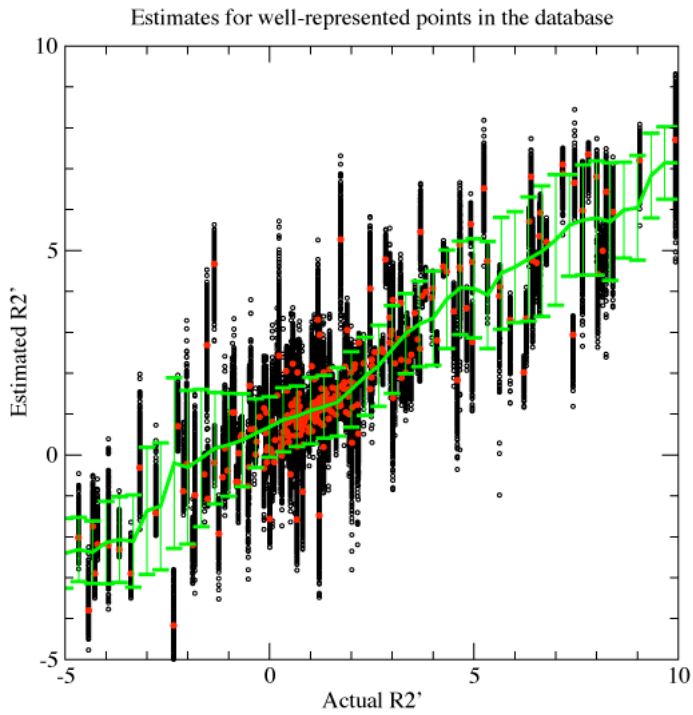
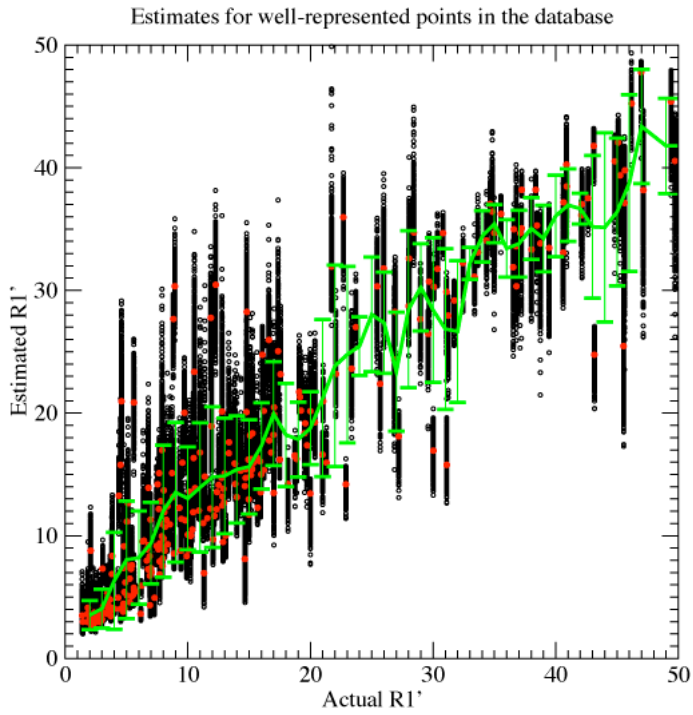


Figure 2. Bayesian estimates of the first two principal components of the precipitation (vertical axis), plotted against the actual values in our May'09 Atlantic ITCZ database (horizontal axis). Estimates were calculated after adding simulated measurement noise to the actual samples (shown in red) in the database.

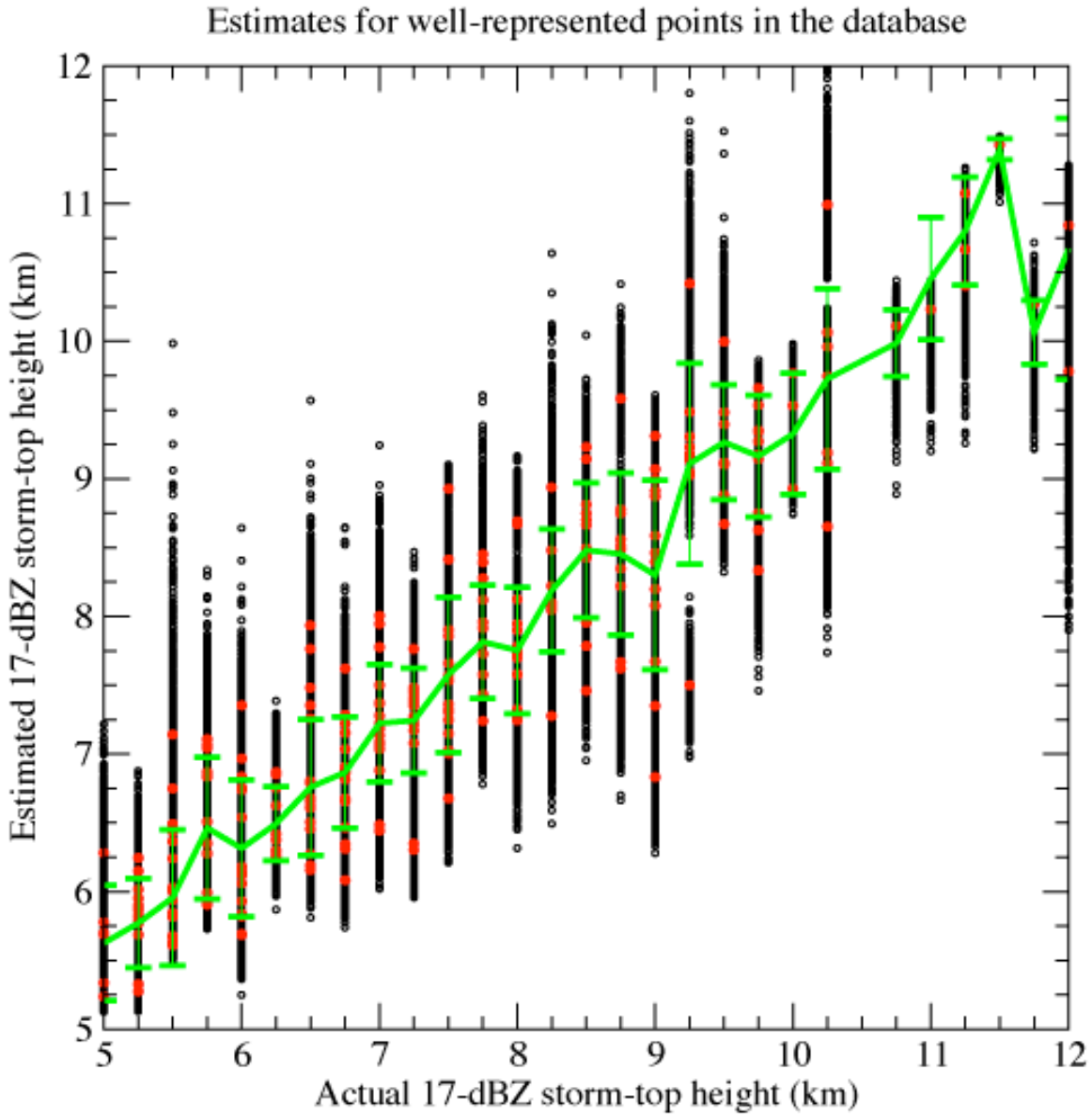


Figure 3. Bayesian estimates of the 17-dBZ storm-top height (vertical axis), plotted against the actual storm-top heights in our May'09 Atlantic ITCZ database (horizontal axis). Estimates were calculated after adding simulated measurement noise to the actual samples (shown in red) in the database.

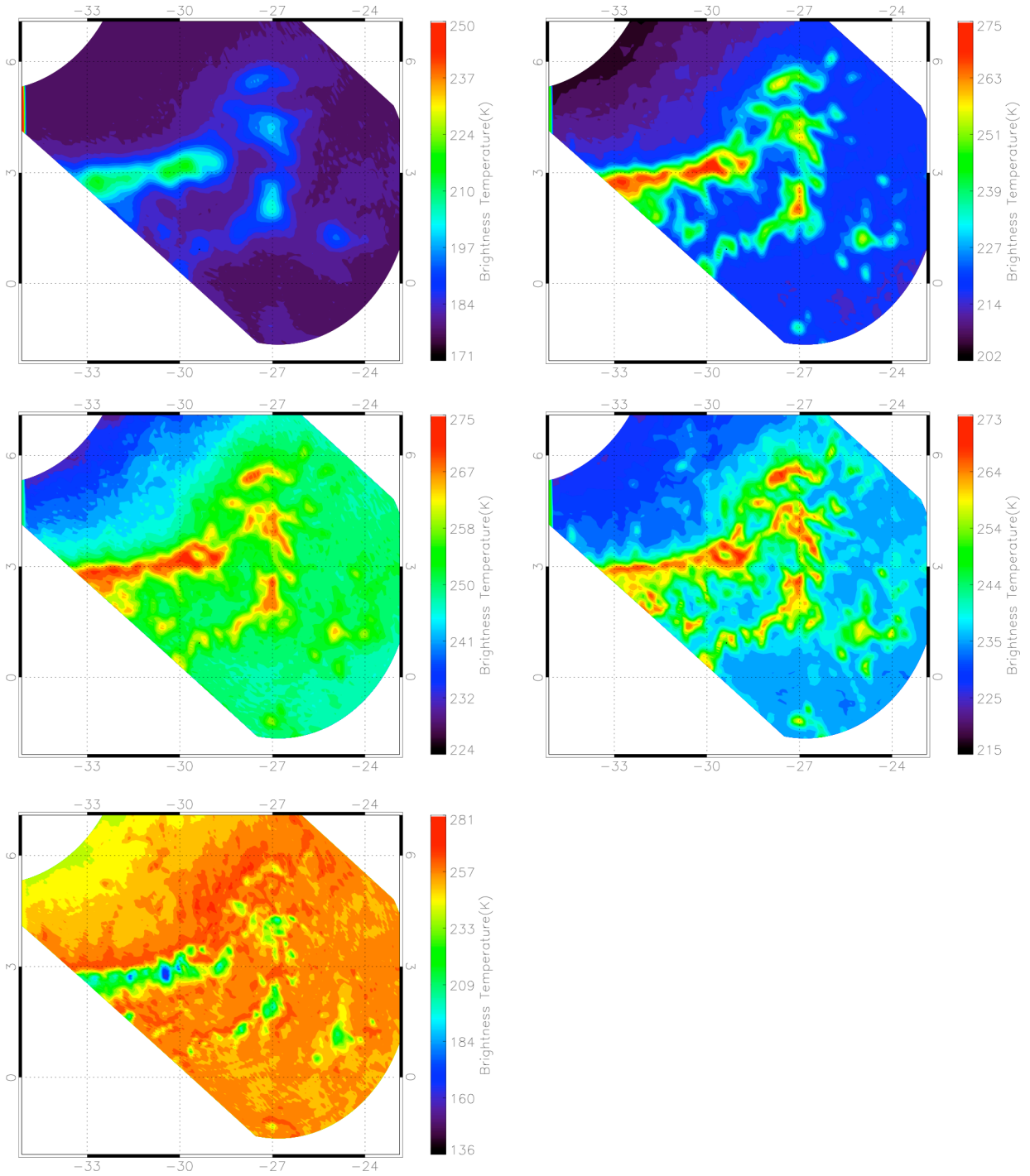


Figure 4. Brightness temperatures measured by the TRMM Microwave Imager on 1 June 2009 at 0230Z during orbit 65760: 10.7GHz-Vpol top left, 19.4GHz-Vpol top right, 21.3V center left, 37GHz-Vpol center right, 85.5GHz-Vpol bottom left.

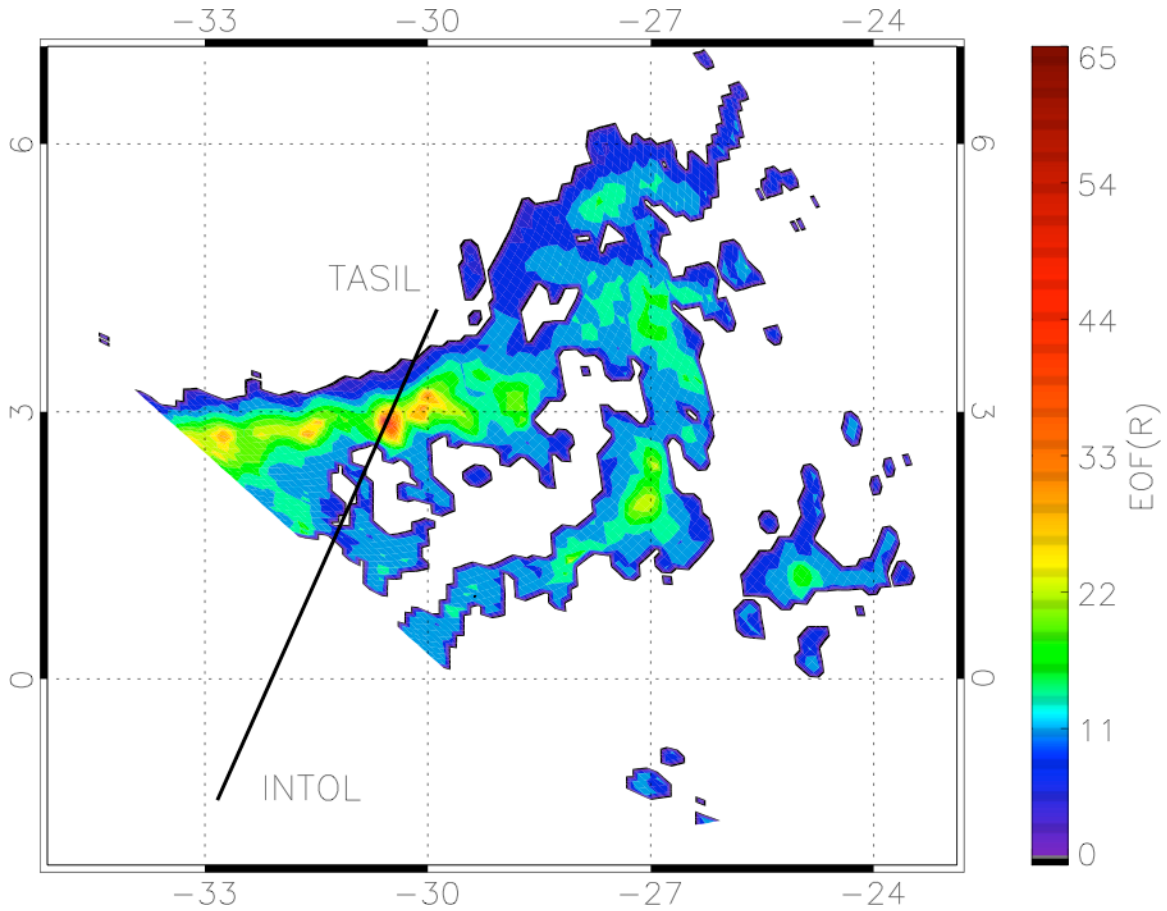


Figure 5. First principal component (essentially 3.5 times the vertical average) of the rain-rate, estimated from TRMM Microwave Imager measurements taken on 1 June 2009 at 0230Z as in figure 4. Flight AF 447 had reached waypoint INTOL at 0133Z and estimated at that time that it would reach waypoint TASIL at 0223Z.

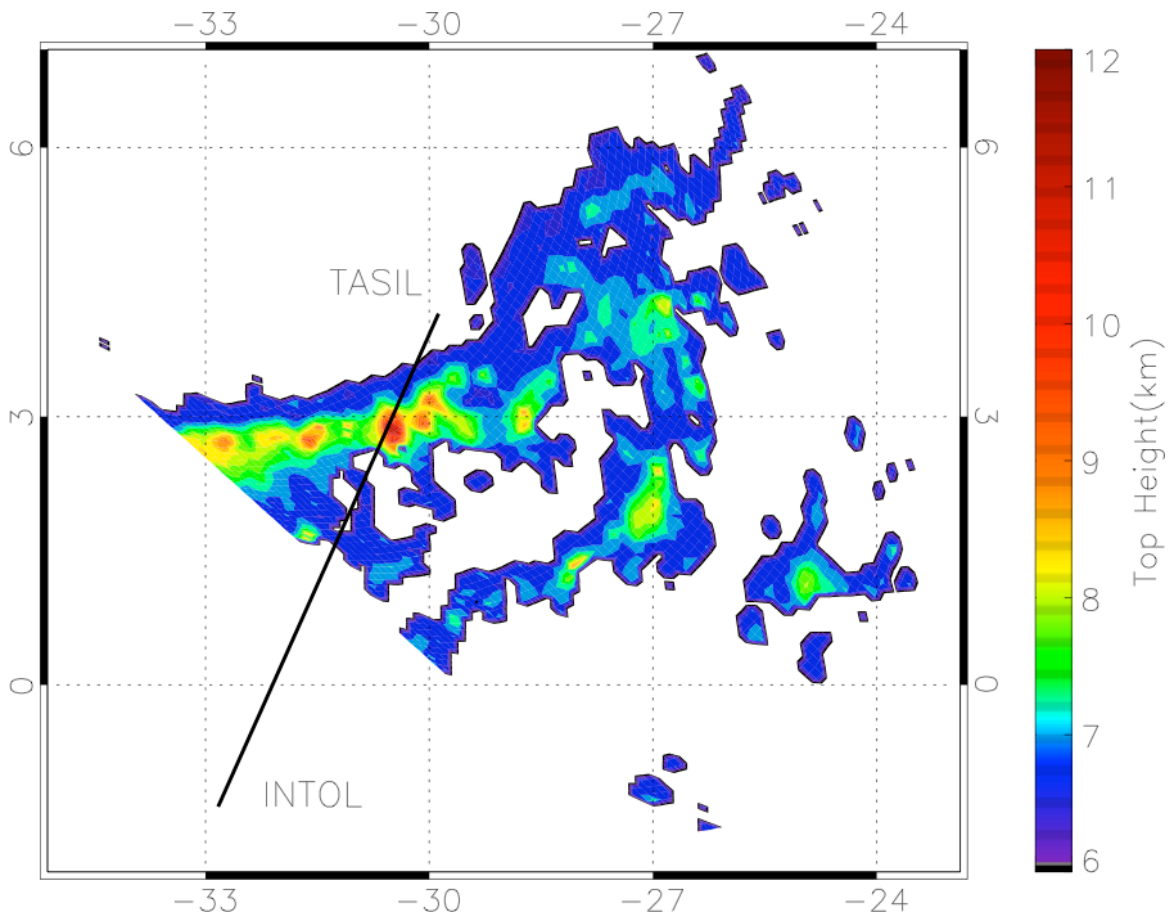


Figure 6. Estimates of the 17-dBZ storm-top heights using the same data as in figures 4 and 5. The last known position of flight AF 447 (BEA, 2009) places the aircraft at 2°58.8'N 30°35.4'W at 02:10Z heading NE.

Tables

$i \setminus j$	9	8	7	6	5	4	3	2	1	0
50	.0003	.0005	.0008	.0009	.0013	.0015	.0018	.002	.0021	.0022
40	.0023	.0028	.0029	.003	.0032	.0034	.0037	.0039	.004	.0041
30	.0044	.0047	.0049	.0053	.0058	.0062	.0066	.0072	.008	.0086
20	.0097	.0107	.012	.0136	.0159	.0179	.0204	.0232	.0272	.0323
10	.0401	.0508	.0653	.0882	.1168	.151	.1901	.2147	.2317	.2523
00	.2616	.2653	.267	.2691	.2682	.2742	.2793	.2784	.2806	.2821

Table 1: Coefficients of the **first precipitation principal component** over the Atlantic ITCZ during May 2009. The coefficient at the row labeled i and the column labeled j applies to the precipitation rate at the 250-m height bin $i+j$, starting at the bin closest to the surface (bin 0) up to the bin whose height extends up to 15000 m (bin 59).

$i \setminus j$	9	8	7	6	5	4	3	2	1	0
50	.0019	.0029	.0044	.0053	.0073	.0084	.0095	.01	.0111	.0115
40	.012	.0135	.0139	.014	.0143	.0156	.016	.0155	.0162	.0164
30	.0172	.0164	.0165	.0184	.0179	.02	.0197	.0218	.0235	.0263
20	.0301	.0307	.0344	.0381	.0416	.0466	.0512	.0566	.064	.0779
10	.0963	.1184	.1478	.1891	.2373	.2724	.325	.3074	.2598	.2212
00	.141	.0782	0	-.0452	-.0891	-.1531	-.2237	-.2758	-.333	-.3803

Table 2: Coefficients of the **second precipitation principal component** over the Atlantic ITCZ during May 2009, with the order as in table 1.

	10V	10H	19V	19H	23V	37V	37H	85V	85H
T_3'	0.225	0.11	0.321	0.287	0.568	-0.102	-0.618	0.02	-0.19
T_4'	0.335	0.627	-0.096	-0.138	-0.273	-0.11	-0.239	0.357	0.441
T_5'	0.363	-0.131	0.26	-0.408	-0.024	0.571	0.056	0.416	-0.339
T_6'	-0.246	-0.097	0.065	0.488	-0.36	-0.214	-0.024	0.641	-0.317
T_7'	0.159	-0.256	0.52	0.216	-0.566	0.16	-0.253	-0.343	0.254
T_8'	-0.6	0.352	0.613	-0.357	0.034	-0.094	0.049	0.017	-0.012
T_9'	0.443	-0.231	0.309	-0.202	0.044	-0.7	0.348	0.056	-0.01

Table 3: Coefficients of the 7 lowest-variability **clear-sky brightness-temperature principal components** over the Atlantic ITCZ during May 2009.